Effect of the interphase microstructure on the behavior of carbon fiber/epoxy resin model composite in a thermal environment

E. Pérez-Pacheco · M. V. Moreno-Chulim ·
A. Valadez-González · C. R. Rios-Soberanis ·
P. J. Herrera-Franco

Abstract The effect of the interfacial microstructure on the stress transfer for a single-fiber carbon fiber/epoxy matrix composite with two different levels of fiber–matrix adhesion for a temperature range between 25 and 115 °C was studied. The heterogeneity of the matrix in the neighborhood of the fiber on the effective mechanical properties of the composite and the possible interactions fiber–matrix that could lead to the development of an interphase dissimilar to the bulk matrix were also analyzed. The preferential absorption of one component of the matrix on the carbon fiber surface is considered to play a key factor on the interfacial behavior for a varying temperature. The matrix-interphase amine-resin stoichiometry is considered to be the main parameter controlling the single-fiber composite behavior when exposed to high temperature.

Introduction

Carbon fiber composites have been widely utilized in advanced applications such as aircraft, aerospace, and military industries resulting in some of them in the exposure to a wide variety of environmental conditions, including temperature and humidity, which are known to have a detrimental effect on the mechanical properties of the matrix, and consequently on the stress transfer capability at the fiber–matrix interface [1–7]. It is known that temperature is one of the factors that can affect the interfacial shear strength (IFSS) of carbon fiber composites even at temperatures below the glass transition temperature (T_g) of the bulk matrix, indicating the formation of an interphase layer of a composition different from that of the bulk matrix [2–6]. Moreover, it has been shown that the microstructure of the matrix in the vicinity of the interphase can be influenced by the proximity of the fiber surface due to changes in reactivity caused by adsorption of matrix components [8–14]. In this study, the temperature dependence on the physicochemical interactions at the interphase of the micromechanical behavior, namely, the fiber–matrix interfacial behavior is presented. In addition, the synergy between the physical, chemical, and mechanical factors that all together contributes to fiber–matrix adhesion and to the fiber–matrix interface strength is revised. This analysis was carried out in a carbon fiber/epoxy matrix composite for a temperature range between 25 and 115 °C and two levels of well-controlled fiber–matrix interfacial properties.

Materials

Intermediate modulus carbon fibers, IM7 12K from Hexcel Co. with an average fiber diameter was 7.0 μm and two different surface conditions were used throughout this study: (1) unsized fibers (untreated, UT) resulting from the commercial sizing removal with a nitric acid treatment, (2) washed fibers and subsequently treated with a silane coupling agent (ST). A Diglycidyl ether of Bisphenol A (DGEBA) based epoxy resin, (Epon 828 from Shell Chemical Company) was used as matrix. Nitric acid (69–71%), ACS and methanol ACS, both reagent grades, from J.T. Baker. Metaphenilene diamine (mPDA) ACS reagent grade was used as a curing agent, and 3-glycidoxy

E. Pérez-Pacheco · M. V. Moreno-Chulim ·
A. Valadez-González · C. R. Rios-Soberanis ·
P. J. Herrera-Franco (✉)
Centro de Investigación Científica de Yucatán, Unidad de Materiales, Calle 43, No. 130, Colonia Chuburná de Hidalgo, 97200 Mérida, YUC, México
e-mail: pherrera@cicy.mx

propyl trimetoxy silane ACS reagent grade from Aldrich Chemical Co as a coupling agent.

Removal of the manufacture's proprietary sizing was done by immersion of tows of the "as-received" carbon fibers in a nitric acid bath for 6 h, heated at 100 °C, then washed until the rinsed water had a neutral pH and dried in a convection oven at 105 °C for 2 h and then, kept in a desiccator. The unsized carbon fibers were subsequently immersed in a 0.1% w/w silane coupling agent aqueous/alcoholic solution (50:50 V/V) and continuously stirred during 1 h. The pH was adjusted to 4 with a diluted acetic acid aqueous solution, and then the fibers were dried in an air convection oven at 120 °C during 2 h, and then placed in a desiccator to await testing.

Experimental procedures

Static and dynamic mechanical properties of the resin as a function of temperature

Mechanical properties of the epoxy resin were determined according to ASTM standard D638 using a Shimadzu Universal testing machine (model AG-I 100 KN) equipped with a 5 kN load cell. A crosshead speed of 5 mm/min was used. For testing at a temperature range from 25 °C up to 115 °C, a specially designed thermal chamber was employed. Determination of the glass transition temperature T_g, the storage modulus, and Tan δ of the epoxy resin was done in a tensile mode using a Q800 TA Instruments Dynamic Mechanical Analyzer (DMA), at a constant frequency of 1 Hz, 0.2 mm amplitude and a heating rate of 5 °C/min.

Fourier transform infrared photo acoustical spectroscopy (FT–IR–PAS) and X-ray photoelectron spectroscopy (XPS) measurements

The Fourier transform infrared photo acoustical spectroscopy (FT–IR–PAS) and the photo-acoustic (PA) spectra associated with the chemical structures of the fibers was studied using a Nicolet model Protege 460 Magna IR spectrometer, equipped with a 8-mm sample cup in a MTEC Model 300 photo acoustic accessory. The spectra were recorded with a 4 cm^{-1} resolution, 60 scans, and a mirror speed of 0.1581 cm s^{-1}. Carbon black, provided by MTEC Photoacoustics Inc., was used as a reference for all the measurements. The cell was purged with ultrapure He (>99.99%) before data collection. Band component analysis was undertaken using the Jandel Peakfit^{TM} software package. Band fitting was done using a Lorentz–Gauss cross-product function. X-ray Photoelectron Spectroscopy (XPS) was performed in a Perkin-Elmer PHI

560/ESCA-SAM system, equipped with a double-pass cylindrical mirror analyzer, with a base pressure of 9.75 × 10^{-10} Torr. Argon ion sputtering was performed with 4-keV energy ions and 0.36 µA cm^{-2} current beams, yielding to about 3 nm min^{-1} sputtering rate. The entire XPS spectra were obtained after 5 min of Ar+ sputtering and for the XPS analysis, the sample was excited with a 1486.60 eV AlKα X-ray. Analysis of the spectra was performed using commercial curve fitting software, Jandel Peakfit^{TM}.

Interfacial shear strength measurement

In order to measure the IFSS, the single-fiber fragmentation test (SFFT) was carried out. In this test, tensile forces are transferred to an embedded single fiber through the interface; with increasing strain the fiber tensile strength is exceeded at some points and breaks repeatedly, resulting in shorter fragments repeatedly until a saturation point is reached; such fragment length is referred to as the critical length L_c [17–19]. The fiber critical length is a good indicator of the ability of the interphase to transmit loads between the two constituents. The ratio (L_c/d) can be used as an indicator of the fiber–matrix bond strength. From this value of the critical length, the IFSS is calculated according to the simple equation [17]:

$$\tau = \frac{\sigma_f}{2}\left(\frac{d}{L_c}\right) \tag{1}$$

where d is the diameter of the fiber, L_c is the critical length of the fiber, and σ_f is its maximum tensile strength. Drzal et al. [13] studied the statistical distribution of fiber fragments lengths and found that it fits well a two-parameter Weibull distribution and rearranged the Kelly and Tyson equation to calculate an average IFSS:

$$\tau = \frac{\sigma_f}{2\beta}\Gamma\left(1 - \frac{1}{\alpha}\right) \tag{2}$$

where, α and β are the shape and scale parameters of the Weibull distribution, respectively, and Γ is the gamma function. The SFFT specimens are made using an eight-cavity molds and 150 mm long fibers selected from a fiber bundle; after being filled with resin, the assembly is transferred to an oven to complete the curing cycle. A constant strain rate of 0.02 mm/min was applied using a Minimat loading frame equipped with a 100 N load cell and mounted on a polarized microscope stage. The L_c was measured in a temperature range between 25 and 115 °C at intervals of 10 °C using an Image XR 2000 Optical Calliper for a gage length of 18 mm and a special Teflon-thermal chamber equipped with a Watlow temperature controller (Series 93).

Results and discussions

As can be observed in Fig. 1, at higher temperatures, the behavior of each of the IFSS differs considerably for each fiber surface treatment. When the temperature reaches approximately 50 °C, an inflection point is noticed for the UT fiber specimens and then, the IFSS slowly decreases. For the ST fiber, the inflection point is noticed after 70 °C. As the temperature is further increased, it can be said that the IFSS remains almost constant for the ST fibers, but for the untreated fibers, another inflection point is noticed at around 95 °C. This behavior defines three regions for the untreated fibers and two regions for the treated fibers in this temperature range.

Mechanical and physico-chemical interactions at the interphase

Since the IFSS is the result of the interactions that take place in the interphase, namely, the mechanical and the physico-chemical interactions, it is necessary to review each of them to further understand the behavior of the single-fiber composite with increasing temperature. The first factor that contributes to the mechanical fiber–matrix interlocking is the state of residual stresses that is built in the specimen [21–23]. First, upon resin curing, there exists a contraction that should result in a radial compressive stress component, uniformly distributed acting along the fiber. This state of stress is referred to as a state of residual stress. Upon loading such initial radial stress component should be further increased by the mechanically induced radial stress caused by the Poisson's ratio radial contraction of the epoxy resin. When the temperature is augmented, the

matrix tends to expand, creating a tensile radial stress which is opposite to the initial compressive radial state of stress, thereby resulting in some stress relief. When loading is applied and the fiber-fragmentation process is initiated, the uniformity of the state of stress is disturbed and the stress distribution along each fiber fragment will change. In order to assess the effect of the residual, thermal and mechanical stress, the micromechanical model proposed by Whitney and Drzal is used [24]. This model offers the possibility of incorporating at the same time all of the stress components mentioned above.

$$\tau_{xy} = -4.75\mu A_1 \varepsilon_0 \bar{x} e^{-4.75\bar{x}} \tag{4}$$

$$\sigma_r = \frac{2k_f G_m}{(k_f + G_m)} A_2 \varepsilon_0 + \mu^2 A_1 (4.75\bar{x} - 1)\varepsilon_0 e^{-4.75\bar{x}} \tag{5}$$

where

$$A_1 = \left\{ E_{1f}\left(1 - \frac{\bar{\varepsilon}_{1f}}{\varepsilon_0}\right) + \frac{4k_f G_m v_{12f}}{(k_f + G_m)} \right.$$
$$\left. \times \left[(v_{12f} - v_m) + \frac{(1 + v_m)\bar{\varepsilon}_m - \bar{\varepsilon}_{2f} - v_{12}\bar{\varepsilon}_{1f}}{\varepsilon_0} \right] \right\} \tag{6}$$

$$A_2 = (v_{12f} - v_m) + \frac{[(1 - v_m)\bar{\varepsilon}_m - \bar{\varepsilon}_{2f} - v_{12f}\bar{\varepsilon}_{1f}]}{\varepsilon_0} \tag{7}$$

And, $\bar{x} = {}^x/_{L_c}$ is the applied far-field strain, μ and K_f given by:

$$\mu = \left(\frac{G_m}{E_{1f} - 4v_{12f}G_m}\right)^{\frac{1}{2}} \text{ and } K_f = \frac{E_m}{2\left(2 - \frac{E_{2f}}{2G_{2f}} - \frac{2v_{12f}^2 E_{2f}}{E_{1f}}\right)} \tag{8}$$

E_{1f} denotes the fiber axial elastic modulus, v_{12f} the longitudinal Poisson's ratio of the fiber, and G_m, denotes the
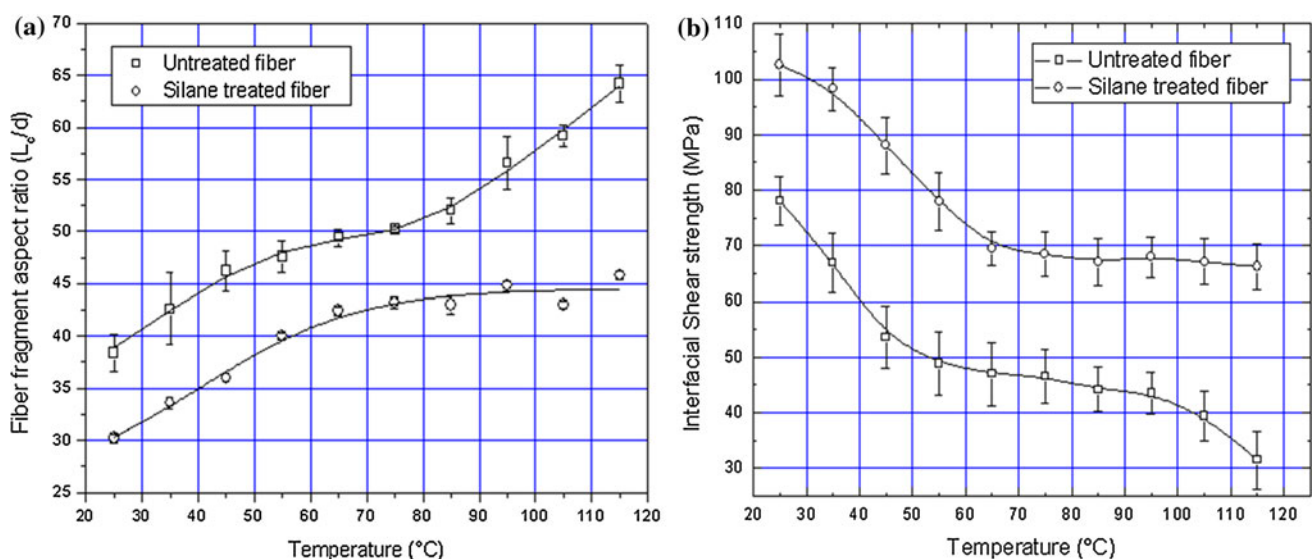

Fig. 1 Critical Fiber aspect ratio and the corresponding interfacial shear stress calculated using the equation proposed by Drzal [24]

matrix shear modulus. Thermal strains are indicated by overbars, E_{2f}, G_{2f}, and K_f are the radial elastic modulus, shear modulus and the plane-strain bulk modulus of the fiber, respectively (Table 1) and E_m is the elastic modulus of the fiber.

In this study the value of α_m was assumed to be constant because it is very small since the resin is assumed to be isotropic, the density at temperature T, ρ_T, is given by $\rho_T = \rho_{T_r}/[1 + 3\alpha(T - T_r)]$ where ρ_{T_r} is the density at room temperature (T_r) and therefore, for the test temperature range, the change of α_m could be considered negligible [20]. It should be pointed out that both μ and K_f are functions of the mechanical properties of the matrix; therefore, they should be changed with temperature as indicated in Fig. 1a. The heterogeneity of the matrix in the neighborhood of the fiber on the effective mechanical properties of the composite has been a subject of continuous study [11, 12]. A number of possible fiber–matrix interactions that could lead to the development of an interphase dissimilar to the bulk matrix have been reported. The preferential absorption of the matrix on one component of the matrix on the carbon fiber surface is considered very important. It has been reported from measurements of the surface energy of epoxy resins and amine hardeners that the amine is preferentially absorbed on the fiber surface. Also, an amine gradient close to the interface produced by matrix dilution of the size was report by Drzal et al. [13]. There are also reports about the carbon fiber surface treatments that include oxidative and non-oxidative methods aimed at the improvement of the adhesion of the carbon fiber to the epoxy resin [14–16]. In general, these techniques attempt to modify the interfacial region by increasing the surface roughness to produce a better mechanical interlocking or by increasing the chemical reactivity of the interface by forming surface functional groups that provide chemical bonding to the matrix. There is also one possible reaction which has relevance to the adhesion between the carbon fiber and the epoxy resin [23]. This is the reaction between amines, acting as nucleophiles, and the vinylic C=C bonds on the carbon fiber surface, acting as electrophiles. This means that immobilization of simple N-alkylamines consumes most of the reactive sites at the carbon fiber surface. As a consequence, the carbon

fiber will not present the proper functionalities to the matrix material to produce good adhesion. This process could also result in a defect of amine groups in the fiber surface neighborhood, and therefore resulting in a variation of the planned epoxy resin-amine curing agent. Therefore, in order to estimate the physico-chemical and mechanical properties of the interface, the bulk resin properties are compared with the interphase resin properties. The dynamical mechanical analysis results for the blends of resin-amine and resin-amine-silane agent are shown in Fig. 2a. It can be noticed that for the stoichiometric relationship epoxy resin-amine (mPDA 14 phr); the Tan δ is approximately at 155 °C. A decrease on the amount of amine groups to react with the resin (mPDA 7 phr) shows a Tan δ at approximately at 95 °C. Additionally, the lack of reaction sites on the fibers could result in differences in the number of possible reaction sites with the silane coupling agent. This will result in a region whose material properties will be completely different to those observed for the bulk matrix. As shown in Fig. 2b, for the amine-deficient stoichiometry a further reduction of the storage modulus is observed. This is opposite to the behavior observed for the 14 phr amine stoichiometry, i.e., a larger amount of silane, which exhibits an increase of the storage modulus.

As shown in Fig. 1b, the IFSS for both UT and ST carbon fibers, decreases monotonically in the range of 25–55 °C, despite the fact that the storage modulus of the epoxy matrix remains almost constant, that is, it decreased less than a 10%. A similar effect should be expected on the mechanical properties of the interfacial region. It has been pointed out that a carbon fiber adsorbs part of the curing amine on its surface thereby affecting the chemical composition of the interphase, because of a stoichiometric imbalance of the epoxy resin in the vicinity of the fiber [8]. However, both crosslink density and T_g decrease for mixtures below or above stoichiometry. Also it should be remembered that the elastic modulus of the resin increases with the number of cross-linked points or equivalently, as its Mc decreases. Then, the drop of the elastic modulus is shifted to higher temperatures [13]. Here, the T_g of the interphase is expected to be close to a temperature of approximately 93 °C and its elastic modulus to be higher than that observed for the bulk matrix, but more susceptible of change with an increasing temperature.

As seen in Fig. 3, the radial stresses resulting from the fragmentation test (calculated using the matrix properties for the 14 phr amine ratio) are very small. In additional, the real contribution of the radial stress component to adhesion should be obtained by multiplying by the coefficient of friction between fiber and matrix, usually estimated at 0.3. Furthermore, because of the temperature increment, practically all the radial stresses are relieved, thus, its contribution to the IFFS, especially after temperatures above

Table 1 Mechanical parameters

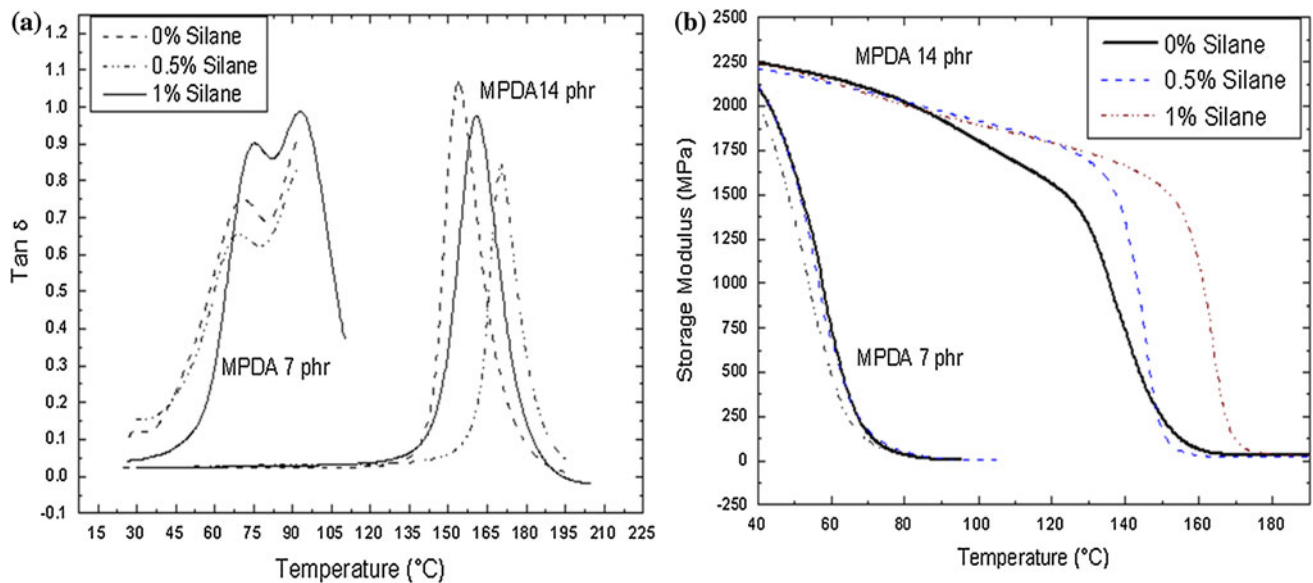| Property	Epoxy	Carbon fiber
E_1 (GPa)	2.04	129
E_2 (GPa)	2.04	21
ν_{12}	0.35	0.25
G_{23} (GPa)	0.75	8.3
α_{12} (10^{-6} °C^{-1})	68	−0.11

Fig. 2 Storage modulus and Tan δ for the epoxy resin cured with the stoichiometric amount of the mPDA curing agent (14 phr) and an unbalanced stoichiometric amount (7 phr) and for model mixtures with silane coupling agent
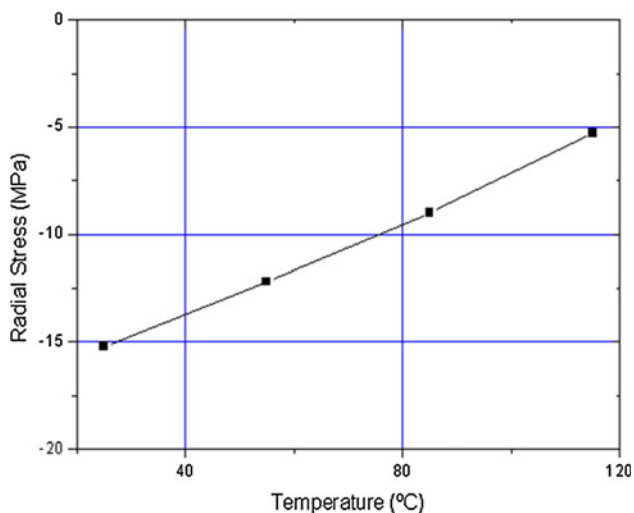

Fig. 3 Peak values for the radial stress as a function of temperature for the 14 phr amine content resin properties

65 °C is negligible. Then, for the UT fibers, any interfacial force transfer will result from frictional interactions between fiber and matrix, and the IFSS will still decrease at higher temperatures. For the ST fibers, there are no signs of fiber–matrix debonding, even for high temperature, and therefore, another mechanism should be responsible for the interface integrity and no sign of any further fiber–matrix debonding. Further, the dependence of the IFSS on the matrix mechanical properties is shown in Fig. 4a and b.

For the 7 phr amine composite, the peak interfacial shear stress rapidly decreases with an increment in temperature, resulting in a loose of fiber–matrix adhesion. This decrement is not as notorious for the 14 phr amine ratio. The peak stresses are plotted for both, the 7 and 14 phr amine ratios (Fig. 5). One important aspect that should be pointed out is the loss of load transfer capacity for untreated fibers at the fiber/matrix interphase when the temperature is augmented above 45 °C in comparison to treated fibers. This can only be attributed to the loss of interfacial mechanical properties. Then, how can the interfacial integrity for the ST fibers or the incomplete debonding for the ST fibers be explained? It is important to remember that in a polymer-matrix composite, besides physical interactions (frictional stresses and mechanical interlocking); there also exist chemical interactions, such as dispersive and acid–base interactions and covalent bonds, contributing to fiber–matrix adhesion.

From the XPS spectra and the deconvolution of electron intensity as a function of the binding energy analysis, for UT and ST carbon fibers, O_{1s} and C_{1s} are the predominant species and occur at 533 and 285 eV, respectively (Fig. 6) [25, 26]. The presence of silicon on the ST fiber surface was detected from its characteristic emission peaks in the region between 150 and 155 eV, for the Si_{2s} and 99–104 eV for the Si_{2p}. Also, for the UT fibers, there are three peaks at 284.9, 286.6, and 288.5 eV that correspond to the aromatic carbon (Car), the carbon in keto-enol equilibrium (C–OH, C–O–C) and the carboxylic groups (C=O, COOH), respectively [27–29] (Fig. 7a). This is an indication of the existence of more than one compound on the UT fiber surface.

The effect of the silane surface treatment is reflected in a shift of the emission peaks. The peak at 284.2 eV has been reported to correspond to the C–Si bond, [28] (Fig. 7b). The peaks at 286.3 and 287.5 eV can be assigned to the
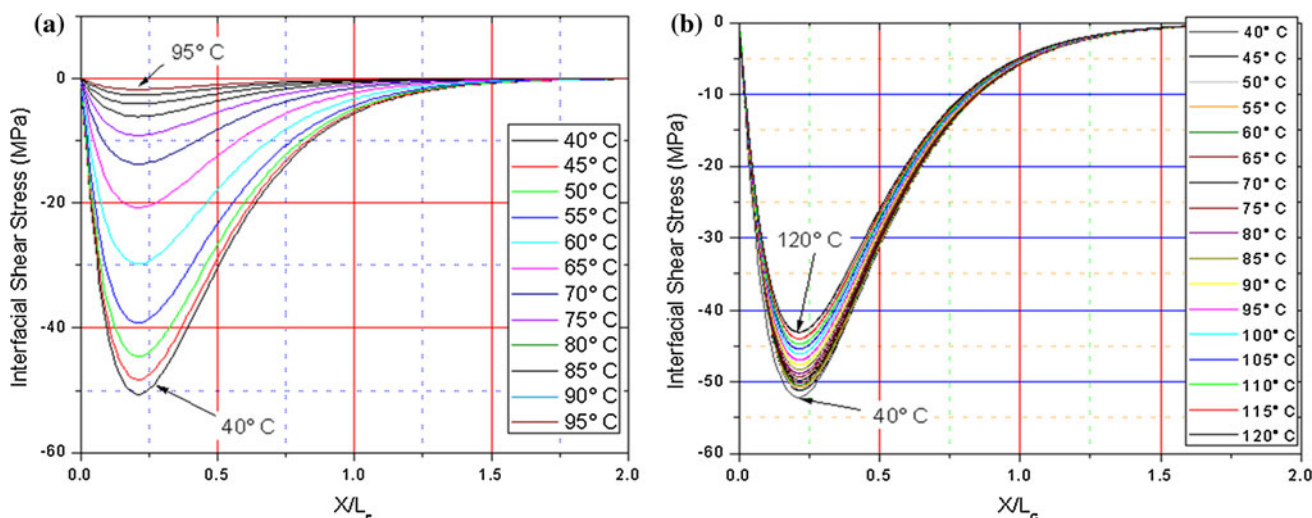
Fig. 4 Shear stress distribution along the fiber fragment length estimated using the Whitmey and Drzal model for **a** 7 amine phr and **b** 14 amine phr
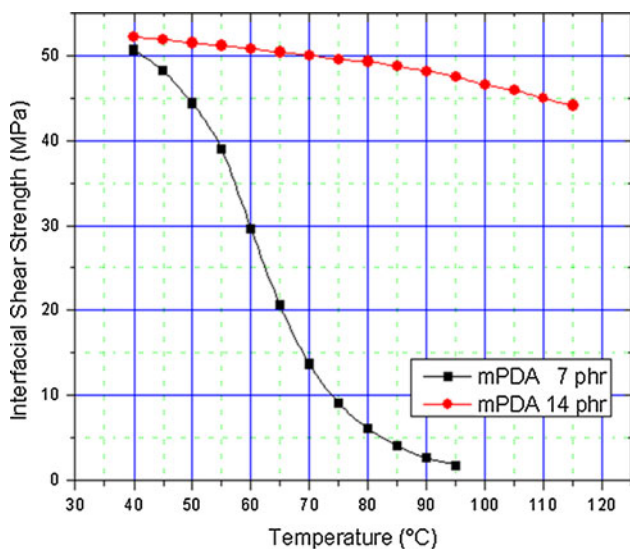

Fig. 5 Peak IFSS estimated using the Whitney and Drzal model for **a** 7 phr amine ratio and **b** 14 phr amine ratio as a function of temperature

Fig. 6 XPS spectra for silane treated and untreated carbon fiber

carbon in keto-enol equilibria (C–OH, C–O–C) and the carboxylic groups (C=O, COOH), respectively. The emission peaks for the O_{1s} (Fig. 8a, b). For the UT fibers, several peaks that correspond to O–C (530.1 eV), COOH (535.9 eV), COC (533.9 eV), and 2C=O (531.5 eV) can be seen, whereas for ST fibers, the presence of the O–Si (532.15 eV), in addition of the peaks found in the UT fiber. In the case of the ST, (Fig. 6), the emission peaks corresponding to the Si_{2S} and Si_{2P} respectively are shown. The peaks at 100, 101.7, and 103.67 eV correspond to the Si–C, Si–OH and Si–O–C bonds, respectively [30–32]. The peak at 153 eV has been assigned to the Si–O bond [25]. These findings seem to confirm the presence of the silane group
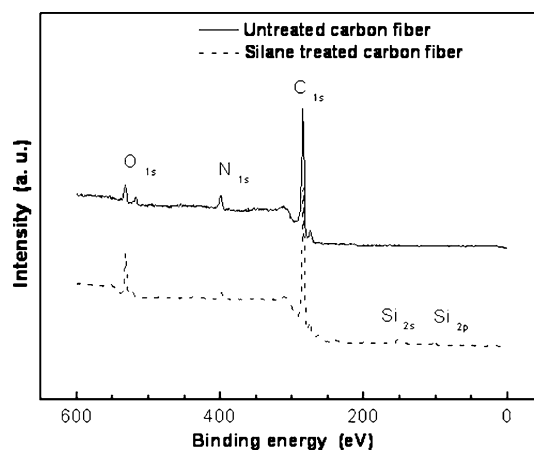
deposited on the surface of the treated fiber. The FTIR spectra for untreated and silane-treated carbon fibers in the 4000–500 cm^{-1} range where the similarity between them can be seen in Fig. 9a. The main differences occur in the range 1600–600 cm^{-1}, (Fig. 9b). In this case, the presence of the asymmetric stretching –Si–O–Si– and/or to the –Si–O–C– bonds [33–35] is noticed. The former bond is indicative of the existence of polysiloxanes deposited on the fiber and the latter confirms the occurrence of a condensation reaction between the silane coupling agent and the carbon fiber. The band at 730 cm^{-1} corresponds the Si–O–Si symmetric stretching that suggests the self-condensation reaction of the hydrolyzed silane to form polysiloxanes. The Si–O–Si bond is confirmed with the band at 1034 cm^{-1}. The band at 815 cm^{-1} has been assigned to the Si–O–C bond [30] and together with the absorptions at 1086 cm^{-1} [30] and 1200 cm^{-1} [33] seems to confirm the reaction between the hydrolyzed silane and the carbon fiber.

Fig. 7 C$_{1S}$ peak emission detected for XPS spectra for **a** untreated and **b** silane treated carbon fiber
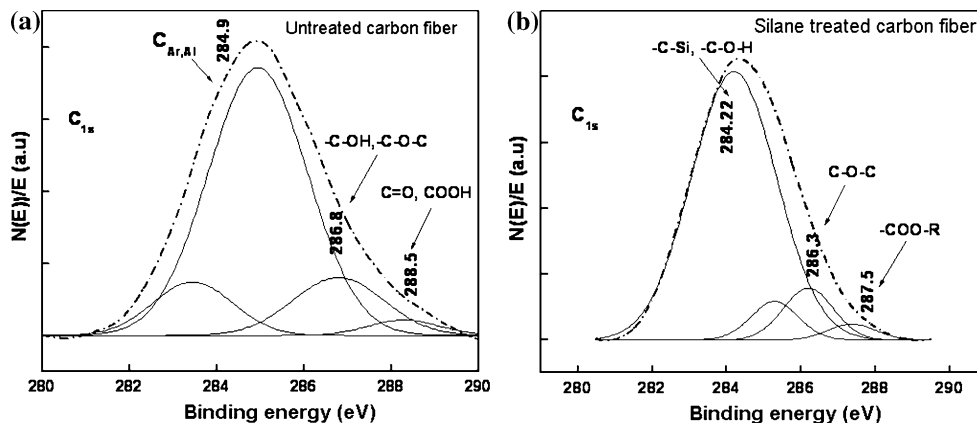

Fig. 8 O$_{1S}$ peak emission detected for XPS spectra for **a** untreated and **b** silane treated carbon fiber
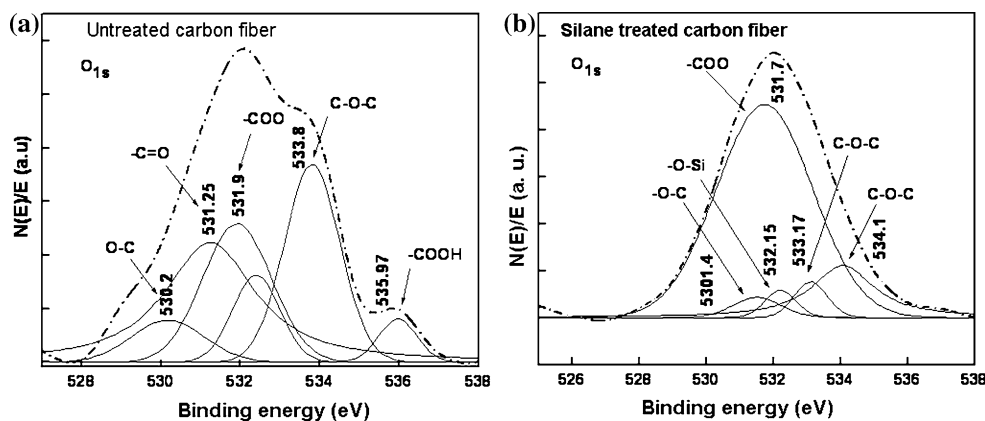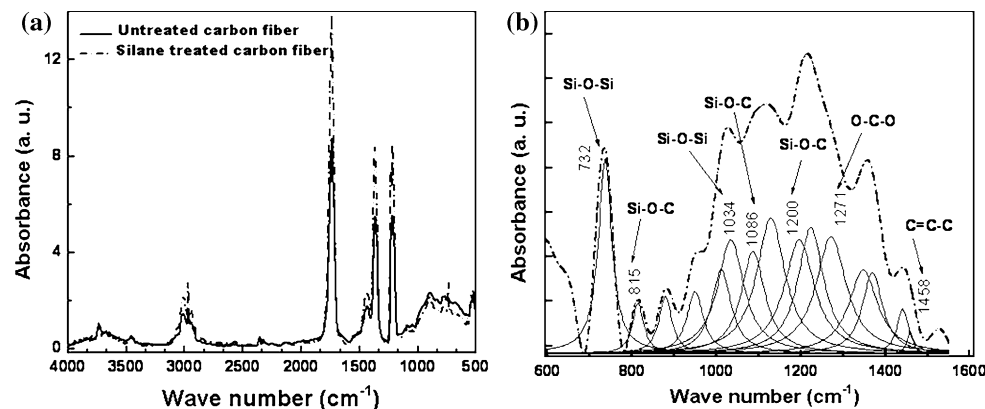

Fig. 9 a FTIR spectra for untreated and silane treated carbon fiber. **b** Spectra differences of FTIR for untreated and silane carbon fibers

Then, the difference in the degree of adhesion observed between the UT and ST fibers above 75 °C is attributed to specific interactions acid–base and covalent bonding at the fiber–matrix interface for the ST fiber, unlike the UT fiber which has no chemical interactions.

Conclusions

The effect of the interfacial microstructure of the fiber–matrix load transfer capability over a temperature range between 25 and 115 °C for a carbon fiber/epoxy matrix composite and two different levels of fiber–matrix adhesion were studied. The physical, chemical and mechanical interactions at the interface and how they contribute to the fiber–matrix load transfer capability were analyzed. The thermal residual stresses, that contribute to the compressive interfacial radial stress play a role on the interface integrity only for temperature values up to 55 °C for the UT carbon fibers, and up to 75 °C for the ST carbon fibers. Above these temperature values, the microstructure of the interface becomes the main factor that contributes to the load

transfer capability. In the case of the UT fibers, besides the low frictional stresses that result from the thermal stresses relief and the weak fiber–matrix physico-chemical interactions, there is a continuous decrement of interface integrity because of the sharp decrease of the mechanical properties of the matrix, E_m due to stoichiometric imbalances in the vicinity of the fiber and as a function of temperature. For the silane treated fiber both frictional stresses and strong covalent bonds are responsible of the fiber–matrix adhesion. Again, as the temperature is increased and the residual stresses were relieved, at certain temperature value (75 °C approximately), believed to be close to the T_g of fiber–matrix interphase, a change in the slope of the IFSS curve was observed. After this, for higher temperature, in spite of the notorious decrease of mechanical properties of both matrix and interphase, there was no evidence of any fiber–matrix interface failure. The strong covalent bonds resulting from chemical reactions on the surface of the fiber are believed to be responsible for the remaining fiber–matrix adhesion and to contribute to the fiber–matrix interphase integrity up to the temperature values studied in this article.

References

1. Ohsawa T, Nakayama A, Miwa M, Hasegawa A (1978) J Appl Polym Sci 22:3203
2. Rao V, Drzal LT (1992) J Adhes 37:83
3. Skourlis TP, McCullough RL (1993) Comp Sci Tech 49:363
4. Detassis M, Pegoretti A, Migliaresi C (1995) Comp Sci Tech 53:39
5. Varelidis PC, McCoullough RL, Papaspyrides CD (1998) Comp Sci Tech 58:1487
6. Walther MB, Reifsnider KL, Madhukar M, Genidy MS (2001) J Comp Tech Res 23:36
7. Cho D, Choi Y, Chang JH, Drzal LT (2006) Comp Interface 13:215
8. Palmese GR, McCullough RL (1992) J Appl Polym Sci 46:1863
9. Kardos JL (1985) In: Proceedings of the symposium on polymer composite: interfaces, held at the American Chemical Society meeting, Seattle Washington. Plenum Press, New York
10. Yang F, Pitchumani R (2004) Comp Sci Tech 64:1437
11. Attwood D, Marshall PI (1996) Comp A 27A:775
12. Fitzer F, Huttner W, Weiss R (1994) Carbon 18:389
13. Drzal LT, Ric MJ, Koenig M, Lloyd P (1983) J Adhes 16:133
14. Montes-Moran Ma, Young RJ (2002) Carbon 40(6):845
15. Montes-Moran Ma, Young RJ (2002) Carbon 40(6):857
16. Montes-Moran MA, Martinez-Alonso A, Tascon JMD, Young RJ (2001) Comp A 32:361
17. Wimolkiatisak AS, Bell JP (1989) Polym Comp 10:162
18. Herrera PJ, Drzal LT (1992) Composites 23(6):2
19. Gupta VB, Drzal LT, Rich MJ (1985) J Appl Polym Sci 30:4467
20. Nielsen LE, Landel RF (1994) Mechanical properties of polymers and composites. Marcel Decker, New York
21. Detassis M, Pegoretti A, Migliaresi C, Wagner D (1996) J Mater Sci 31:2385. doi:10.1007/BF01152951
22. Gerard G, Gilbert AC (1957) J Appl Mech (ASME) 24:355
23. Quek MY (2004) Int J Adhes Adhes 24:379
24. Whitney JM, Drzal LT (1987) ASTM STP 937, American Society for Testing and Materials, pp 179–196
25. Wagner CD, Riggs WM and Muilenberg GE (1978) Handbook of X-ray photoelectron spectroscopy. Perkin Elmer Corporation, Eden Prairie
26. Beamson G, Briggs D (1992) High resolution XPS of organic polymers. The Scienta ESCA300 Database. Wiley, Chichester
27. Xie Y, Sherwood PM (1990) Chem Mater 2:293
28. Pamula E, Rouxhet PG (2003) Carbon 41:1905
29. Zielke U, Huttinger KJ, Hoffman WP (1996) Carbon 34:983
30. Jing SY, Lee HJ, Choi CK (2002) J Korean Phys Soc 41:769
31. Morra M, Ochiello E, Garbassi F (1993) J Appl Polym Sci 48:1331
32. Toth A, Bertóti I, Blazso M, Bánhegyi G, Bognar A, Szaplonczay P (1994) J Appl Polym Sci 52:1293
33. Britcher L, Kehoe D, Matisons J, Swincer G (1995) Macromolecules 28:3110
34. Gulyás J, Rosenberger S, Földes E, Pukanszky B (2000) Polym Compos 21:387
35. Farhadyar N, Rahimi N, Langroundi AE (2005) Iran Polym J 14:155